



HAL
open science

Highly oxygenated isoprenylated cyclohexanoids from the fungus *Parastagonospora nodorum* SN15

Amr El-Demerdash, Grégory Genta-Jouve, Margot Bärenstrauch, Caroline Kunz, Emmanuel Baudouin, Soizic Prado

► To cite this version:

Amr El-Demerdash, Grégory Genta-Jouve, Margot Bärenstrauch, Caroline Kunz, Emmanuel Baudouin, et al.. Highly oxygenated isoprenylated cyclohexanoids from the fungus *Parastagonospora nodorum* SN15. *Phytochemistry*, 2019, 166, pp.112056 -. 10.1016/j.phytochem.2019.112056 . hal-03487373

HAL Id: hal-03487373

<https://hal.science/hal-03487373>

Submitted on 20 Dec 2021

HAL is a multi-disciplinary open access archive for the deposit and dissemination of scientific research documents, whether they are published or not. The documents may come from teaching and research institutions in France or abroad, or from public or private research centers.

L'archive ouverte pluridisciplinaire **HAL**, est destinée au dépôt et à la diffusion de documents scientifiques de niveau recherche, publiés ou non, émanant des établissements d'enseignement et de recherche français ou étrangers, des laboratoires publics ou privés.



Distributed under a Creative Commons Attribution - NonCommercial 4.0 International License

Highly oxygenated isoprenylated cyclohexanoids from the fungus

Parastagonospora nodorum SN15

Amr El-Demerdash,^{1,2} Grégory Genta-Jouve,^{1,3} Margot Bärenstrauch,¹ Caroline Kunz,^{1,4} Emmanuel Baudouin,⁵ Soizic Prado^{1*}

¹Muséum National d'Histoire Naturelle, Unité Molécules de Communication et Adaptation des Micro-organismes, UMR 7245, CP 54, 57 rue Cuvier, 75005 Paris, France

²Organic Chemistry Division, Chemistry Department, Faculty of Science, Mansoura University, Mansoura 35516, Egypt

³Université Paris Descartes, Laboratoire de Chimie-Toxicologie Analytique et Cellulaire (C-TAC), UMR CNRS 8638, COMETE, 4 Avenue de l'Observatoire 75006 Paris, France

⁴Sorbonne Université, Faculté des Sciences et Ingénierie, UFR 927, F-75005 Paris, France

⁵Sorbonne Université, CNRS, Laboratoire de Biologie du Développement, Institut de Biologie Paris Seine (LBD-IBPS), Paris F-75005, France

Abstract: The chemical investigation of the wheat plant pathogen *Parastagonospora nodorum* SN15 led to the purification of seven highly oxygenated acetylenic cyclohexanoids named stagonosporynes A-H (**1-7**). Their structures were determined on the basis of extensive NMR and the relative and absolute configurations by an array of computational methods including simulation of NOESY spectrum and electronic circular dichroism (ECD). All compounds were evaluated for their herbicidal activity and stagonosporyne G (**7**) displayed the most significant herbicidal activity.

1 **1. Introduction**

2 The Dothideomycetes represent a large and diverse class of fungi including many plant
3 pathogens. Dothideomycetes are also prolific producers of specialised metabolites
4 (Chomcheon et al., 2006; Chomcheon et al., 2009; Hewage et al., 2014; Senadeera et al.,
5 2012), which may be required for pathogenicity (Muria-Gonzalez et al., 2015; Stergiopoulos
6 et al., 2013). Among members of Dothideomycete plant pathogens, *Parastagonospora*
7 *nodorum* (Teleomorph: *Phaeosphaeria*, syn. *Septoria*) is known as the causative agent of
8 *Stagonospora* (or *Septoria*) *nodorum* blotch leading to major losses in wheat crops in many
9 parts of the world (Figueroa et al., 2018; Solomon et al., 2006). Accordingly, *P. nodorum* has
10 emerged as a Dothideomycete necrotrophic pathogen model and has been sequenced in 2007
11 (Hane et al., 2007). Its genome revealed the presence of 38 specialised metabolite
12 biosynthetic gene clusters (BGC) including genes coding for polyketide synthases (PKS);
13 non-ribosomal peptide synthases (NRPS), terpene synthases and prenyl transferases
14 suggesting a strong potential of specialised metabolite production (Chooi et al., 2014; Ipcho et
15 al., 2012).

16 Interestingly, the authors showed that the expression of several BGCs was upregulated
17 during *in planta* infection (Ipcho et al., 2012) such as *SNOG_00477* and *SNOG-5791-5797*
18 gene clusters. Deletion of *SN477* gene combined with its heterologous expression in
19 *Saccharomyces cerevisiae* revealed that it encodes for a PR-PKS responsible of the
20 biosynthesis of (*R*)-(-)-mellein, a well know dihydroisocoumarine compound previously
21 described as phytotoxic and widely widespread in fungi (Arakawa, 1968; Blair and Newbold,
22 1955; Chooi et al., 2015; Nishikawa, 1933). Recently heterologous expression of *SNOG-*
23 *5791-5797* in *Aspergillus nidulans* led to the isolation of new phytotoxic α -pyrones (Li et al.,
24 2018). Previous chemical investigations of *P. nodorum* led also to the identification of several
25 other metabolites (Devys et al., 1994; Devys et al., 1992; Tan et al., 2009; Yang et al., 2013)
26 but their number remains quite low compared to the huge biosynthetic potential of the strain.

27 Accordingly, and as a part of our ongoing research program on fungal natural products,
28 we investigated the chemistry of the fungus *Parastagonospora nodorum* SN15 cultivated on
29 rice medium. This led to the identification of seven previously undescribed highly oxygenated
30 cyclohexanoids named stagonosporynes A-G (**1-7**) along with the known compound siccayne
31 (**8**) (Figure 1). Herein we report their isolation and structural elucidation along with their
32 herbicidal activity.

33

35 **2. Results and discussion**

36 Molecular formula of compound **1** was established as C₁₁H₁₆O₃ from its positive
37 HRESIMS *m/z* 219.0984 [M+Na]⁺ (calc. for C₁₁H₁₆O₃Na 219.0997), indicating four
38 unsaturation degrees. The IR spectrum exhibited characteristic absorption bands for hydroxyl
39 functionalities (3443 cm⁻¹). The ¹³C-*J* modulated NMR spectrum recorded in CDCl₃ revealed
40 the resonance of 11 carbons including one methyl at (δ_C 23.4, CH₃-11), two oxymethines at
41 (δ_C 74.3, C-1; δ_C 65.7, C-4), three methylenes (δ_C 25.9, C-2; δ_C 31.9, C-3; δ_C 44.1, C-5) and
42 one olefinic carbon at (δ_C 122.9, C-10). Three quaternary resonances including two acetylenic
43 carbons (δ_C 89.7, C-7 and δ_C 85.6, C-8) and one sp² carbon (δ_C 125.7, C-9) along with one
44 oxygenated sp³ carbon at (δ_C 70.6, C-6) were also depicted (**Table 3**). Taking into account the
45 four degrees of unsaturation elucidated from the HRMS, compound **1** must be cyclic. The ¹H
46 NMR spectrum recorded in CDCl₃ (**Table 1**) revealed the presence of two oxymethine
47 protons (δ_H 3.72, H-1; δ_H 3.97, H-4) and three methylenes (δ_H 1.83/1.68, CH₂-2; δ_H 1.95/1.35,
48 CH₂-3; δ_H 2.38/1.66, CH₂-5) suggesting an oxygenated cyclohexanoid scaffold. Additional
49 signals for two olefinic protons CH₂-10 observed at δ_H 5.24/5.29 and a terminal methyl CH₃-
50 11 at δ_H 1.86 suggested a methyl-terminal double bond function. ¹H-¹H COSY spectrum
51 recorded in DMSO-*d*₆ of **1** revealed the presence of one main spin-coupling system showed in
52 bold blue lines (**Figure 2**), including the oxygenated methine CH-1 (δ_H 3.72), the two
53 methylenes groups CH₂-2 and CH₂-3 (δ_H 1.83/1.68, δ_H 1.35/1.95), the oxymethine CH-4 (δ_H
54 3.97) and the methylene CH₂-5 (δ_H 1.66/2.38). The ¹H-¹H COSY spectrum allowed us to
55 identify a second substructure including a terminal methyl (δ_H 1.86, CH₃-11) with the olefinic
56 protons (δ_H 5.24 and 5.29, CH₂-10). These two substructures were assembled together based
57 on the cross-peaks correlations observed in HMBC. Indeed, the oxymethine H-1 (δ_H 3.72) and
58 the two diastereotopic protons CH₂-5 (δ_H 1.66/2.38) displayed key HMBC correlations
59 (**Figure 2**) with C-6 (δ_C 76.5) confirming that **1** is a cyclohexane-containing compound.
60 Additional key HMBC correlations (**Figure 1**) were observed between the olefinic protons
61 CH₂-10, the terminal methyl CH₃-11 and the acetylenic carbone C-8 (δ_C 85.6). Furthermore,
62 both H-1 and CH₂-5 displayed HMBC correlations with the acetylenic quaternary carbon C-7
63 (δ_C 89.7) indicating the connection of the enyne unit at C-6. This was further confirmed by
64 key HMBC correlations observed in DMSO-*d*₆ between OH-6 (δ_H 4.89) and the quaternary
65 carbon C-7 (δ_C 89.3). The relative configuration of **1** was deduced from the values of the

66 proton coupling constants and the NOESY correlations. NOEs observed in DMSO-*d*₆ and
67 CDCl₃ between H-4 and H-5eq/H-3eq and H-2ax suggest that they are in the same plan.
68 Additionally, NOEs between H-1 and H-3ax, H-5ax and H-2-eq suggest that there are on the
69 other side of the cyclohexane ring. Relative configuration at C-6 was deduced from NOEs
70 observed in DMSO-*d*₆ between OH-6 and H-4, H-5eq (Figure 2). This was confirmed by
71 *trans*-diaxial coupling constants observed on ¹H-spectrum (CDCl₃) *J*_{a/a} 10.6 H-1/H-2ax and
72 10.1 H-4/H-3ax, which established that H-1 and H-4 were in axial position of a chair
73 conformation for the cyclohexane ring (Figure 3). Therefore, compound **1** was assigned as
74 shown (Figure 1) and named stagonosporyne A. To determine the absolute configuration of
75 **1**, prediction of the ECD spectrum was undertaken and the experimental and simulated
76 spectra generated by time-dependent density functional theory (TDDFT) were compared. All
77 computational works were performed using Gaussian 16 (Frisch et al., 2016). The absolute
78 configuration of **1** was determined as 1*S*, 4*S*, 6*S* as the only Cotton effect (due to the π→π*
79 transition of the enyne moiety) depicted on the spectra shared the same sign (Figure 4).

80 Molecular formula of compound **2** was established as C₁₁H₁₆O₄ from its positive HR-
81 ESI-MS *m/z*. 235.09319 [M+Na]⁺ (calcd. for C₁₁H₁₆O₄Na 235.0946), indicating four
82 unsaturation degrees. The IR spectrum exhibited distinct absorption bands for hydroxyl
83 functionalities (broad band at 3369 cm⁻¹). The NMR spectral data of **2** recorded in both
84 DMSO-*d*₆ and CD₃OD showed similar features of a highly oxygenated cyclohexanoid
85 compound. The obvious difference was the presence of an oxymethine in C-5 at δ_H 2.95/δ_C
86 79.5 (DMSO-*d*₆) instead of the methylene CH₂-5 at δ_H 2.06/1.38 and δ_C 46.7 previously
87 described for stagonosporyne A (**1**). Compound **2** was thus named stagonosporyne B. The
88 relative configuration of **2** was deduced based on the proton coupling constant values and
89 NOESY correlations. The *trans*-diaxial coupling constants observed on ¹H-NMR spectrum
90 (CD₃OD) (*J*_{a/a} 9.4, 11.4, 11.8) of H-5/H-4, H-4/H-3ax and H-2ax/H-1 allowed us to assign H-
91 1, H-5 and H-4 in axial form of a chair conformation for the cyclohexane ring. Moreover,
92 NOEs observed in DMSO-*d*₆ between H-1 and H-5/OH-6/H-3ax suggest that they are in the
93 same plan while NOEs between H-4 and H-2ax/OH-5 suggest that there are on the other side
94 of the six-membered ring (Figure 3). Accordingly, structure **2** was determined as shown in
95 (Figure 1). The absolute configuration of **2** was determined as 1*R*, 4*R*, 5*S*, 6*S* by comparison
96 of the ECD spectrum with the one obtained for compound **1** (only one CE observed for this
97 family of compounds).

98 The molecular formula C₁₃H₁₈O₅ was established for compound **3** according its
99 HRESIMS [M+K]⁺ *m/z* 293.0796 (Calc. for C₁₃H₁₈O₅K 293.0791) and indicates five degrees

100 of unsaturation. Comparison of the ^1H NMR spectrum (**Table 1**) of **3** with this one of **2**
101 indicated that the both compounds are closely related structures. Indeed, the only differences
102 were the presence of an extra methyl signal (δ_{H} 2.05, δ_{C} 21.1, 3H, CH_3 -13) along with the
103 carbonyl C-12 (δ_{C} 172.7), which was attributed to an acetyl functionality CH_3CO and satisfied
104 the fifth unsaturation degree suggested by the HRMS. This was further confirmed through key
105 HMBC correlations from both the oxymethine H-4 (δ_{H} 4.81, 1H) and CH_3 -13 (δ_{H} 2.05, 3H),
106 with the quaternary carbonyl ester at (δ_{C} 172.7, C-12) allowing thus to define the attachment
107 of the acetyl group at C-4 (**Figure 2**). The relative stereochemistry was determined from the
108 NOESY spectroscopy. The NOEs correlations between H-1/H-5/H-3ax and H-2eq suggested
109 that there are on the same side, whereas further NOEs correlations between H-4/H-2ax/H-3eq
110 indicated that there are in the opposite side. In addition, the large coupling constant ($J_{4/5} = 9.9$
111 Hz) between the two oxymethines H-4 and H-5 indicated that these protons are in a *trans*-
112 diaxial orientation. Furthermore, the large coupling constant ($J_{1/2} = 11.8$ Hz) between H-1 and
113 H-2ax suggested also that H-1 is in axial position. In order to confirm the relative
114 configuration of **3**, we took advantage of the recently introduced software package Spinach
115 (Edwards et al., 2014; Hogben et al., 2011). Following a classical procedure used for DP4
116 calculations, namely, geometry optimization followed by frequency calculations, NMR
117 properties were calculated using the Gaussian 16W software using density functional theory
118 at the B3LYP/STO-3G level for all eight diastereoisomers (Figure S34 *supporting*
119 *information*, compound **3** a-h). In order to stick to the experimental NOESY spectrum, all the
120 parameters (spectral window, magnet strength, number of points and mixing time) were set as
121 for the data acquisition. To facilitate the comparison between experimental and theoretical
122 spectra, the Zeeman interactions were defined as scalars from the experimental data. The
123 identification of the right relative configuration was then deduced using a “spot the
124 difference” approach between experimental NOESY and simulated one. As shown Figure
125 S34, the *1R*,4R*,5R*,6R*-3a* was ruled out based because of the two differences observed,
126 the absence of crosspeak between H-1/H-3ax and the additional cross-peak between H-10b/H-
127 13. The diastereoisomers **3-b**, **3-d**, **3-f** and **3-h** were dismissed because of the absence of
128 crosspeaks H1/H-3ax and H-5/H-3ax together with the presence H-5/H-3eq. The
129 diastereoisomer **3-c** was discarded based on the absence of crosspeak corresponding to the H-
130 1/H-3ax. Eventually, **3-e** was excluded due to the absence of the intense crosspeak H10a/H-13
131 on the experimental spectrum. The relative configuration was then assigned as
132 *1S*,4S*,5R*,6R*-3*. This approach was further confirmed by the proton couplings similar to

133 compound **2**. The absolute configuration of **3** was also determined as 1*R*, 4*R*, 5*S*, 6*S* as both
134 experimental and calculated ECD spectra nicely looked alike (**Figure S82**, *supporting*
135 *information*). Therefore, the structure **3** was established and named stagonosporyn C (**3**).

136 The molecular formula C₁₂H₁₄O₅ was determined for compound **4** according to its HR-
137 ESI-MS *m/z* 237.0755 [M-H]⁻ (calc. 237.0763), suggesting six degrees of unsaturation. The IR
138 spectrum exhibited characteristic absorption bands at 3378 and 1790 cm⁻¹ for hydroxyl and
139 carbonate carbonyl functionality. The ¹³C NMR spectrum (**Table 3**) of **4** exhibited 12 carbon
140 resonances consisting of one sp³ methyl CH₃-11 (δ_C 22.9), two sp³ methylenes CH₂-2 (δ_C
141 24.9) and CH₂-3 (δ_C 20.9), three sp³ oxymethines CH-1 (δ_C 73.6), CH-4 (δ_C 78.9) and CH-5
142 (δ_C 82.9), one oxygenated sp³ carbon C-6 (δ_C 73.2), one sp² methine CH₂-10 at (δ_C 123.4),
143 two sp² carbons C-9 and C-12 corresponding to an olefinic one and a carbonate carbonyl at
144 (δ_C 127.6) and (δ_C 157.6), respectively. Two sp acetylenic C-7 and C-8 carbons at (δ_C 86.7)
145 and (δ_C 90.1), respectively were also depicted on ¹³C NMR. The ¹H NMR and ¹H-¹H COSY
146 data (**Table 1** & **Figure 2**) of **4** suggested that this compound is also an isoprenylated
147 cyclohexanoid structurally related to the aforementioned stagonosporyne A (**1**) except for the
148 presence of an additional carbonate carbonyl carbon at δ_C 157.6. This cyclic carbonate
149 functionality was further confirmed by HMBC correlations observed between both
150 oxymethine protons H-4 (δ_H 4.95) and H-5 (δ_H 4.72) with the carbon C-12 (δ_C 157.6)
151 establishing the carbonate moiety at C-4 and C-5. Therefore compound **4** was assigned as a
152 carbonate derivative of compound **1**. NOEs correlation between H-4, H-5, H₂-ax and H-3_{eq}
153 suggested that these protons are orientated on the same side and confirmed the *cis* relationship
154 between H-4 and H-5. This conclusion was confirmed by the coupling constant (*J*_{4/5} = 6.5)
155 between H-4 and H-5 suggesting a torsion angle of ca 40° between these two protons. In
156 addition, coupling constant of H-1 (*J*_{e/a} 4.9, *J*_{e/e} 1.5) suggested that H-1 is in equatorial
157 position. The relative configuration was assigned using the NOESY simulation (**Figure S42**,
158 *supporting information*) approach described above and the 1*S**, 4*R**, 5*R**, 6*S** configuration
159 could be assigned for **4**. The absolute configuration was determined by comparison of the sign
160 of the unique CE on the ECD spectrum with the other compounds (**Figure S82**, *supporting*
161 *information*). Structure **4** was thus elucidated as the stagonosporyne D.

162 Molecular formula C₁₂H₁₂O₅ was established to Stagonosporyne E (**5**) according to its
163 negative HR-ESI-MS at *m/z* 235.0593 [M-H]⁻ (235.0606 calcd. for C₁₂H₁₁O₅), indicating
164 seven degrees of unsaturation. The ¹³C and ¹H NMR data as well 2D NMR spectral data
165 interpretation including ¹H-¹H COSY, ¹H-¹³C HSQC and HMBC (**Figure 2**) indicated that

166 compound **5** displays similar framework as deduced before for stagonosporyne D (**4**). The key
167 difference between the two compounds was the replacement of the two methylenes CH₂-2 and
168 CH₂-3 in **4** by an *endo*-cyclic double bond suggesting a 1,4,5,6-tetraoxygenated cyclohexene
169 ring system. This observation was consistent with the molecular formula determined by
170 HRMS. The relative configuration was deduced from NOESY and ¹H NMR coupling
171 constants analyses. Indeed, the coupling constant $J_{1/2} = 5.0$ Hz suggested that H-1 is in
172 *pseudo*-equatorial position. The coupling constants $J_{4/5} = 7.6$ Hz as well as the NOE
173 correlations between H-4 and H-5 characterized their *cis* relationship. The NOE correlation
174 observed between H1/H5-ax on the NOESY simulation spectra (**Figure S51, supporting**
175 *information*) confirmed the *1S**, *4R**, *5R**, *6S**-**5**. In agreement with the relative configuration
176 of **4**. The ECD spectrum was similar to the one obtained for **5** thus the absolute configuration
177 was assigned accordingly. The structure for compound **5** was proposed and named
178 stagonosporyne E.

179 The molecular formula of compound **6** was determined as C₁₁H₁₄O₃ according to its
180 negative HR-ESI-MS at m/z 193.0854 [M-H]⁻, which requires five double bond equivalents.
181 Examination of its ¹H and ¹³C NMR data (**Table 2 & 3**) indicated the presence of a 1,4,6-
182 trihydroxy cyclohexene core bearing an *endo*-cyclic double bond at C2-C3 at (δ_H 5.52/5.75,
183 δ_C 129.8/133.4 respectively), satisfying the fifth unsaturation degree. The COSY in
184 combination with HSQC, HMBC (**Figure 2**) supported the identification of structure **6** as the
185 stagonosporyn F (**Figure 1**). The analysis of its ¹H NMR spectrum (**Table 2**) showed that the
186 large coupling constant ($J_{4/5} = 9.4$ Hz) between H-4 and H-5ax suggests that there are in
187 *trans*-diaxial position while the coupling constant ($J_{1/2} = 2.1$ Hz) between H-1 and H-2
188 suggests that H-1 is in *pseudo*-axial position. This was further confirmed by key NOEs
189 correlations between H-4 and H-5eq and H-1 and H-5ax and NOESY simulation spectra
190 (**Figure S60, supporting information**). The absolute configuration was thus assigned as *1S**,
191 *4R**, *6S**-**6**.

192 Compound **7** was purified in minute quantity (0.5 mg). It displayed a molecular
193 formula C₁₁H₁₄O₃ at m/z 193.0854, [M-H]⁻, established by HRESIMS, indicating five
194 unsaturation degrees. The ¹H NMR and ¹³C (**Table 2 & 3**) of **7** displayed similarities with
195 those recorded for stagonosporyne F (**6**). Indeed, the key difference was the presence of an
196 additional oxymethine H-5 (δ_H 3.41, δ_C 75.6) and as well as a sp³ methine H-6 (δ_H 2.62, δ_C
197 45.3) instead of the hydroxylated carbon C-6, previously observed for compound **6**. The
198 COSY spectrum (**Figure 1**) revealed the presence of a main spin system from H-1 to H-6

199 corresponding to a 1,4,5-tri-oxygenated cyclohexene system. The HMBC spectrum (**Figure 2**)
200 displayed key correlations that confirmed this motif. Indeed, the two oxymethines H-1 (δ_{H}
201 4.20) and H-5 (δ_{H} 3.41) exhibited HMBC correlations with the methine C-6 at (δ_{C} 45.3).
202 Further key HMBC correlations were observed from both H-5 (δ_{H} 3.41) and H-6 (δ_{H} 2.62)
203 with the quaternary carbon C-7 at δ_{C} 88.8, confirming the attachment of an isoprenyl side
204 chain at C-6. The ^1H NMR spectrum (**Table 2**) showed characteristic large coupling constants
205 ($J_{5/6}$ 11.4, $J_{5/4}$ 8.0 and $J_{6/1}$ 9.3 Hz) suggesting that H-1 and H-6 as well as H-4 and H-5 are in
206 *trans* diaxial positions. This was further confirmed by strong NOE correlations between H-1
207 and H-5 as well as between H-4 and H-6. Based on all previously mentioned spectral data,
208 structure **7** was therefore assigned as stagonosporyne G (**7**). The ECD spectrum was similar to
209 the one obtained for **5** thus the absolute configuration was assigned *1S*, *4S*, *5S*, *6R*
210 accordingly.

211 Compound **8** was purified as pale yellow oil material. It had a molecular formula
212 $\text{C}_{11}\text{H}_{11}\text{O}_2$, established by HRESIMS at m/z 175,0747 $[\text{M}+\text{H}]^+$ (calcd for 175,0754), indicating
213 seven degrees of unsaturation. A preliminary investigation of its ^1H NMR spectrum showed
214 characteristic signals of a 1,2,4-trisubstituted benzene ring, consisting of a *meta*-coupled
215 proton H-1 (δ_{H} 6.70, *d*, 2.7) and two *ortho*-coupled aromatic protons H-3 (δ_{H} 6.64, *dd*, 8.6,
216 2.7) and H-4 (δ_{H} 6.67, *d*, 8.6). The full extensive 2D NMR spectral data analysis involving
217 COSY, HSQC and HMBC support the identified structure **8** as siccayne, a previously isolated
218 compound from the marine fungi *Halocyphina villosa* (Kupka et al., 1981).

219 The acetylenic containing metabolites display a myriad of important biological
220 activities

221 (Kuklev et al., 2013) and among them herbicidal and antimicrobial ones that have already
222 been reported. Especially phomentrioloxin B, an acetylenic polyoxygenated cyclohexene
223 structurally related to our isolated compounds and previously isolated from the fungus
224 *Diaporthe gulayae* caused necrotic spots on *Papaver rhoes* and *Urtica dioica* at 5mM (Andolfi
225 et al., 2014). Furthermore, closely related compounds were isolated from the Australian native
226 grass, *Neurachne alopecuroidea* and showed *in vitro* growth promotion of barley seedlings
227 and potent activity against several phytopathogens such as *Phytophthora cinnamomi*,
228 *Rhizoctonia salona*, *Pythium irregular* and *Alternaria alternata*.

229 Accordingly, the pure isolated natural products stagonosporyne A-G (**1-7**) along with
230 siccayne (**8**) were tested for their herbicidal and antifungal activities. Stagonosporynes A-G
231 (**1-7**) did not display antifungal activity against the two phytopathogens *Fusarium oxysporum*
232 and *Botrytis cinerea* (data not shown). Stagonosporynes A-F (**1-6**) did not exhibit herbicidal

233 activity while stagonosporyne G (7) displayed a significant herbicidal activity at the highest
234 tested concentration (100 µg/mL) against the laboratory model plant *Arabidopsis thaliana* as
235 shown in **Figure 5**.

236 **3. Conclusion**

237 The chemical investigation of the wheat plant pathogen *Parastagonospora nodorum* SN15
238 led to the purification of seven highly oxygenated acetylenic cyclohexanoids named
239 stagonosporynes A-H (1-7). All compounds were evaluated for their herbicidal activity and
240 stagonosporyne G (7) displayed the most significant herbicidal activity. Thus, taken together,
241 these results suggest that stagonosporyne G may belong to the chemical arsenal required for
242 the virulence of *P. nodorum* SN15. Further experiments are therefore needed to determine the
243 precise role of this compound in *P. nodorum* wheat colonization.

244 **4. Experimental.**

245 *4.1. General Experimental Procedures.*

246 Optical rotations $[\alpha]^{20}_D$ were determined using a Perkin Elmer 341 polarimeter. IR
247 spectra were performed on a PerkinElmer BX FR-IR spectrometer. The CD spectra were
248 finished on Jasco J-810 spectropolarimeter system. High-resolution mass spectra were
249 recorded on an API Q-STAR PULSAR i of Applied Biosystem by direct injection of the
250 purified compounds. 1D and 2D NMR spectra were recorded on Bruker Avance III HD 400
251 MHz and 600 MHz spectrometers (Wissembourg, France) equipped with a BBFO Plus Smart
252 probe and a triple resonance TCI cryoprobe, respectively (CNRS-MNHN). The chemical
253 shifts are relative to the residual signal solvent (CD₃OD: δ_H 3.31; δ_C 49.15; CD₃CN: δ_H 1.94;
254 δ_C 118.26, CDCl₃: δ_H 7.26; δ_C 77.16; DMSO-*d*₆: δ_H 2.50; δ_C 39.52). Preparative HPLC
255 experiments were performed on an Agilent system and an Agilent PrepHT XDB-C18 column
256 (21.2 × 150 mm i.d.; 5 µm; USA). Column chromatography (CC) was performed using silica
257 gel (Geduran Si 60, 40–63 µm, Merck, Germany and Lichroprep RP-18, 40–63µm, Merck
258 KGaA, Germany); TLC silica gel-precoated plates (F254, 20 × 20 cm, Merck KGaA,
259 Germany).

260 *4.2. Microorganism.*

261 The fungus *Parastagonospora nodorum* SN15 was grown in 5L Erlenmeyer flasks (5
262 x 600 mL inoculated with 5mL fungal suspension in glycerol 10%) at 25 °C for 21 days under
263 a 12 h photoperiod culturing parameters.

264 4.3. *Extraction and isolation.*

265 The rice culture of the fungus *Parastagonospora nodorum* SN15 was extracted by 2 L
266 of ethyl acetate. Organic phases were combined and dried over anhydrous MgSO₄, filtrated
267 and concentrated under reduced pressure to afford 19 g of brown gummy material. The
268 methanolic soluble part (4.75 g) was subjected to a normal phase silica-gel flash
269 chromatography (35-70 μm), using a gradient of cyclohexane/ CH₂Cl₂ [100/0→0/100]. The
270 column was further eluted using a gradient of CH₂Cl₂/MeOH [100/0→0/100] and terminated
271 with ethyl acetate/acetone/water/formic acid (5/3/0.5/0.5) to afford 25 fractions. All fractions
272 were monitored by TLC using different eluent systems and combined together according to
273 their polarities in 13 major fractions F1-F13. Promising fractions F8, F9 and F10 were
274 introduced for further reparative chromatographic purifications by reversed phase
275 (preparative/semi-preparative and analytical C₁₈-HPLC) using the eluent system
276 water/acetonitrile containing 0.1% formic acid. The detailed isolation scheme of the isolated
277 compounds and their quantities is given in the supporting information.

278 4.4. *Computational details.*

279 All Density functional theory calculations were performed using Gaussian 16W. After
280 a conformational analysis with the GMMX module and the MMFF94 force field ($\Delta E < 1.5$
281 kcal/mol), a geometry optimization was realized at the B3LYP/STO-3G level. Rotational
282 strength was calculated using TD DFT at the B3LYP/6.31g level for 20 excited states. Total
283 nuclear spin-spin coupling J (Hz) were predicted at the B3LYP/STO-3G level. Zeeman
284 interactions were defined as scalars from the experimental data.

285 4.5. *Biological activities.*

286 Surface sterilized *Arabidopsis thaliana* Columbia-0 seeds were sown in 96-well plates
287 (4-5 seeds per well) and incubated at 22°C under continuous light, in the presence of 200 μL
288 half-strength Murashige and Skoog (MS) medium (Duchefa, France). After 5 days, MS
289 medium was removed and replaced by 200 μL of fresh medium supplemented with
290 stagonosporine G dissolved in DMSO. For all conditions, the final concentration of DMSO
291 represented 1% of the total volume of medium. For glyphosate controls, a ready-to-use
292 commercial solution of Roundup[®] containing 7.2 g.L⁻¹ of acid glyphosate was diluted in MS
293 medium to a final concentration of 72μg.mL⁻¹. Plantlets were photographed after 7 days and
294 survival rate was established as the percentage of fully-green plantlets over the total number
295 of developed seedlings.

296 4.6. Analytical data of isolated compounds

297 Stagonosporyne A (**1**): colorless oil (1.2 mg); $[\alpha]_D^{20} + 6$ ($c = 0.80$, MeOH), ECD (0.8
298 mg/mL, MeOH); IR (neat) ν_{\max} 3443, 2955, 2925, 2870, 1725, 1463, 1384, 1270, 1122, 1073,
299 741 cm^{-1} ; ^1H NMR and ^{13}C NMR, **Table 1 and 3**; HRESIMS m/z 219.0682 $[\text{M}+\text{Na}]^+$ (calcd
300 for $\text{C}_{11}\text{H}_{16}\text{O}_3\text{Na}$, 219.0678).

301 Stagonosporyne B (**2**): colorless oil (1.6 mg); $[\alpha]_D^{20} + 10$ ($c = 1.06$, MeOH), ECD (0.8
302 mg/mL, MeOH); IR (neat) ν_{\max} 3369, 2922, 2853, 1716, 1601, 1455, 1395, 1384 cm^{-1} ; ^1H
303 NMR and ^{13}C NMR, **Table 1 and 3**; HRESIMS m/z 235.09319 $[\text{M}+\text{Na}]^+$ (calcd for
304 $\text{C}_{11}\text{H}_{16}\text{O}_4\text{Na}$, 235.0940).

305 Stagonosporyne C (**3**): colorless oil (1.3 mg); $[\alpha]_D^{20} + 14$ ($c = 0.86$, MeOH); ECD (0.65
306 mg/mL, MeOH); IR (neat) ν_{\max} 3383, 2923, 2854, 1716, 1601, 1455, 1395, 1384, 1373 cm^{-1} ;
307 ^1H NMR and ^{13}C NMR, **Table 1 and 3**; HRESIMS m/z 293.0796 $[\text{M}+\text{K}]^+$ (calcd for
308 $\text{C}_{13}\text{H}_{18}\text{O}_5\text{K}$, 293.0785).

309 Stagonosporyne D (**4**): colorless oil (2 mg); $[\alpha]_D^{20} + 26$ ($c = 1.33$, MeOH); ECD (0.66
310 mg/mL, MeOH); IR (neat) ν_{\max} 3378, 2923, 2855, 1790, 1733, 1602, 1445, 1395, 1384, 1373,
311 1265, 1196 cm^{-1} ; ^1H NMR and ^{13}C NMR, **Table 1 and 3**; HRESIMS m/z 237.0755 $[\text{M}-\text{H}]^-$
312 (calcd for $\text{C}_{12}\text{H}_{13}\text{O}_5$, 237.0768).

313 Stagonosporyne E (**5**): colorless oil (1.2 mg); $[\alpha]_D^{20} + 24$ ($c = 0.8$, MeOH); ECD (0.8
314 mg/mL, MeOH); IR (neat) ν_{\max} 3372, 2922, 2853, 1733, 1601, 1455, 1395, 1373, 1255, 1099
315 cm^{-1} ; ^1H NMR and ^{13}C NMR, **Table 1 and 3**; HRESIMS m/z 235.0593 $[\text{M}-\text{H}]^-$ (calcd for
316 $\text{C}_{12}\text{H}_{11}\text{O}_5$, 235.0611).

317 Stagonosporyne F (**6**): pale yellow oil (2.4 mg); $[\alpha]_D^{20} + 67$ ($c = 1.60$, MeOH); ECD (0.24
318 mg/mL, MeOH); IR (neat) ν_{\max} 3347, 2926, 1613, 1374, 1266, 1054, 838 cm^{-1} ; ^1H NMR and
319 ^{13}C NMR, **Table 2 and 3**; HRESIMS m/z 193.0854 $[\text{M}-\text{H}]^-$ (calcd for $\text{C}_{11}\text{H}_{14}\text{O}_3$, 193.0870).

320 Stagonosporyne G (**7**): colorless oil (0.5 mg); $[\alpha]_D^{20} + 18$ ($c = 0.16$, MeOH); ECD (0.5
321 mg/mL, MeOH); IR (neat) ν_{\max} 3343, 2924, 1602, 1448, 1395, 1384, 1373, 1196, 1098, 1035,
322 700 cm^{-1} ; ^1H NMR and ^{13}C NMR, **Table 2 and 3**; HRESIMS m/z 193.0854 $[\text{M}-\text{H}]^-$ (calcd for
323 $\text{C}_{11}\text{H}_{14}\text{O}_3$, 193.0870).

324 **Acknowledgements**

325 This work was supported by ATM “Microorganisms” grant from the Natural History Museum
326 of Paris. The 400 MHz and 600 MHz NMR spectrometers used in this study were funded
327 jointly by the Région Ile-de-France, the MNHN (Paris, France) and the CNRS (France).

328

329 **Références**

330 Andolfi, A., Maddau, L., Basso, S., Linaldeddu, B. T., Cimmino, A., Scanu, B., Deidda, A.,
331 Tuzi, A., Evidente, A., 2014. Diplopimarane, a 20-nor-ent-pimarane produced by the oak
332 pathogen *Diplodia quercivora*. J. Nat. Prod. 77, 2352-2360.

333 Arakawa, H., 1968. Absolute configuration of mellein. Bull. Chem. Soc. Jap. 41, 2541.

334 Blair, J., Newbold, G. T., 1955. The structure of mellein. Chem. Ind. (London, U. K.), 93-94.

335 Chomcheon, P., Sriubolmas, N., Wiyakrutta, S., Ngamrojanavanich, N., Chaichit, N.,
336 Mahidol, C., Ruchirawat, S., Kittakoop, P., 2006. Cyclopentenones, scaffolds for organic
337 syntheses produced by the Eendophytic fungus mitosporic Dothideomycete sp. LRUB20. J
338 . Nat. Prod 69, 1351-1353.

339 Chomcheon, P., Wiyakrutta, S., Sriubolmas, N., Ngamrojanavanich, N., Mahidol, C.,
340 Ruchirawat, S., Kittakoop, P., 2009. Metabolites from the endophytic mitosporic
341 *Dothideomycete* sp. LRUB20. Phytochemistry 70, 121-127.

342 Chooi, Y. H., Krill, C., Barrow, R. A., Chen, S., Trengove, R., Oliver, R. P., Solomon, P. S.,
343 2015. An in planta-expressed polyketide synthase produces (*R*)-mellein in the wheat
344 pathogen *Parastagonospora nodorum*. Appl. Environ. Microbiol. 81, 177-186.

345 Chooi, Y. H., Muria-Gonzalez, M. J., Solomon, P. S., 2014. A genome-wide survey of the
346 secondary metabolite biosynthesis genes in the wheat pathogen *Parastagonospora*
347 *nodorum*. Mycology 5, 192-206.

348 Devys, M., Barbier, M., Bousquet, J.-F., Kollmann, A., 1994. Isolation of the (-)-(3*R*)-5-
349 hydroxymellein from the fungus *Septoria nodorum*. Phytochemistry 35, 825-826.

350 Devys, M., Barbier, M., Kollmann, A., Bousquet, J.-F., 1992. N-Methoxy septorinol, a
351 substituted pyrazine from the fungus *Septoria nodorum*. Phytochemistry 31, 4393-4394. .

352 Edwards, L. J., Savostyanov, D. V., Welderufael, Z. T., Lee, D., Kuprov, I., 2014. Quantum
353 mechanical NMR simulation algorithm for protein-size spin systems. J. Magn. Reson. 243,
354 107-113. .

355 Figueroa, M., Hammond-Kosack, K. E., Solomon, P. S., 2018. A review of wheat diseases—a
356 field perspective. Mol. Plant Pathol. 19, 1523-1536. .

357 Frisch, M. J., Trucks, G. W., Schlegel, H. B., Scuseria, G. E., Robb, M. A., Cheeseman, J. R.,
358 Scalmani, G., Barone, V., Petersson, G. A., Nakatsuji, H., Li, X., Caricato, M., Marenich,
359 A. V., Bloino, J., Janesko, B. G., Gomperts, R., Mennucci, B., Hratchian, H. P., Ortiz, J.
360 V., Izmaylov, A. F., Sonnenberg, J. L., Williams, Ding, F., Lipparini, F., Egidi, F., Goings,
361 J., Peng, B., Petrone, A., Henderson, T., Ranasinghe, D., Zakrzewski, V. G., Gao, J., Rega,
362 N., Zheng, G., Liang, W., Hada, M., Ehara, M., Toyota, K., Fukuda, R., Hasegawa, J.,
363 Ishida, M., Nakajima, T., Honda, Y., Kitao, O., Nakai, H., Vreven, T., Throssell, K.,
364 Montgomery Jr., J. A., Peralta, J. E., Ogliaro, F., Bearpark, M. J., Heyd, J. J., Brothers, E.
365 N., Kudin, K. N., Staroverov, V. N., Keith, T. A., Kobayashi, R., Normand, J.,
366 Raghavachari, K., Rendell, A. P., Burant, J. C., Iyengar, S. S., Tomasi, J., Cossi, M.,
367 Millam, J. M., Klene, M., Adamo, C., Cammi, R., Ochterski, J. W., Martin, R. L.,
368 Morokuma, K., Farkas, O., Foresman, J. B., Fox, D. J., 2016. Gaussian 16 Rev. B.01.
369 Wallingford, CT.

370 Hane, J. K., Lowe, R. G., Solomon, P. S., Tan, K. C., Schoch, C. L., Spatafora, J. W., Crous,
371 P. W., Kodira, C., Birren, B. W., Galagan, J. E., Torriani, S. F., McDonald, B. A., Oliver,
372 R. P., 2007. Dothideomycete plant interactions illuminated by genome sequencing and
373 EST analysis of the wheat pathogen *Stagonospora nodorum*. *Plant Cell* 19, 3347-3368. .

374 Hewage, R. T., Aree, T., Mahidol, C., Ruchirawat, S., Kittakoop, P., 2014. One strain-many
375 compounds (OSMAC) method for production of polyketides, azaphilones, and an
376 isochromanone using the endophytic fungus *Dothideomycete* sp. *Phytochemistry* 108, 87-
377 94. .

378 Hogben, H. J., Krzystyniak, M., Charnock, G. T., Hore, P. J., Kuprov, I., 2011. Spinach--a
379 software library for simulation of spin dynamics in large spin systems. *J. Magn. Reson.*
380 208, 179-194. .

381 Ipcho, S. V., Hane, J. K., Antoni, E. A., Ahren, D., Henrissat, B., Friesen, T. L., Solomon, P.
382 S., Oliver, R. P., 2012. Transcriptome analysis of *Stagonospora nodorum*: gene models,
383 effectors, metabolism and pantothenate dispensability. *Mol. Plant Pathol.* 13, 531-545.

384 Kuklev, D. V., Domb, A. J., Dembitsky, V. M., 2013. Bioactive acetylenic metabolites.
385 *Phytomedicine* 20, 1145-1159.

386 Kupka, J., Anke, T., Steglich, W., Zechlin, L., 1981. Antibiotics from basidiomycetes. XI.
387 The biological activity of siccayne, isolated from the marine fungus *Halocyphina villosa* J.
388 & E. Kohlmeyer. *J. Antibiot. (Tokyo)* 34, 298-304.

389 Li, H., Hu, J., Wei, H., Solomon, P. S., Vuong, D., Lacey, E., Stubbs, K. A., Piggott, A. M.,
390 Chooi, Y. H., 2018. Chemical ecogenomics-guided discovery of phytotoxic alpha-Pyrone
391 from the fungal wheat pathogen *Parastagonospora nodorum*. *Org. Lett.* 20, 6148-6152.

392 Muria-Gonzalez, M. J., Chooi, Y. H., Breen, S., Solomon, P. S., 2015. The past, present and
393 future of secondary metabolite research in the Dothideomycetes. *Mol. Plant. Pathol.* 16, 92-
394 107.

395 Nishikawa, E., 1933. Biochemistry of molds. II. A metabolic product of *Aspergillus melleus*
396 Yukawa. *Nippon Nogei Kagaku Kaishi* 9, 772-774.

397 Senadeera, S. P. D., Wiyakrutta, S., Mahidol, C., Ruchirawat, S., Kittakoop, P., 2012. A novel
398 tricyclic polyketide and its biosynthetic precursor azaphilone derivatives from the
399 endophytic fungus *Dothideomycete* sp. *Org. Biomol. Chem.* 10, 7220-7226.

400 Solomon, P. S., Lowe, R. G., Tan, K. C., Waters, O. D., Oliver, R. P., 2006. *Stagonospora*
401 *nodorum*: cause of stagonospora nodorum blotch of wheat. *Mol. Plant. Pathol.* 7, 147-156.

402 Stergiopoulos, I., Collemare, J., Mehrabi, R., De Wit, P. J., 2013. Phytotoxic secondary
403 metabolites and peptides produced by plant pathogenic *Dothideomycete* fungi. *FEMS*
404 *Microbiol. Rev.* 37, 67-93.

405 Tan, K.-C., Trengove, R. D., Maker, G. L., Oliver, R. P., Solomon, P. S., 2009. Metabolite
406 profiling identifies the mycotoxin alternariol in the pathogen *Stagonospora nodorum*.
407 *Metabolomics* 5, 330-335.

408 Yang, X.-L., Awakawa, T., Wakimoto, T., Abe, I., 2013. Induced biosyntheses of a novel
409 butyrophenone and two aromatic polyketides in the plant pathogen *Stagonospora*
410 *nodorum*. *Nat. Prod. Bioprospect.* 3, 141-144.

411

412

413

414

415

416

417

418

419

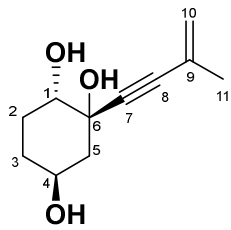
420

421

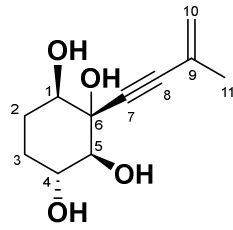
422

423

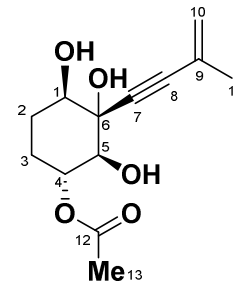
424



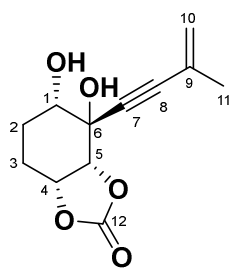
Stagonosporyne A (1)



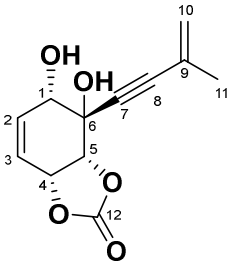
Stagonosporyne B (2)



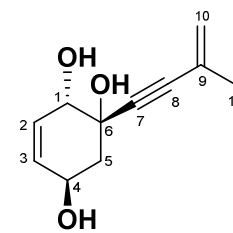
Stagonosporyne C (3)



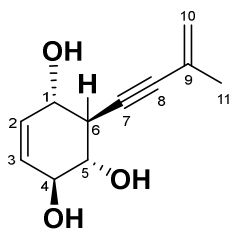
Stagonosporyne D (4)



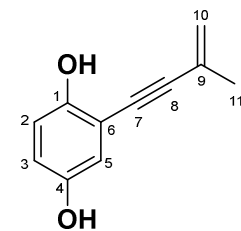
Stagonosporyne E (5)



Stagonosporyne F (6)



Stagonosporyne G (7)



Siccayne (8)

Figure 1.

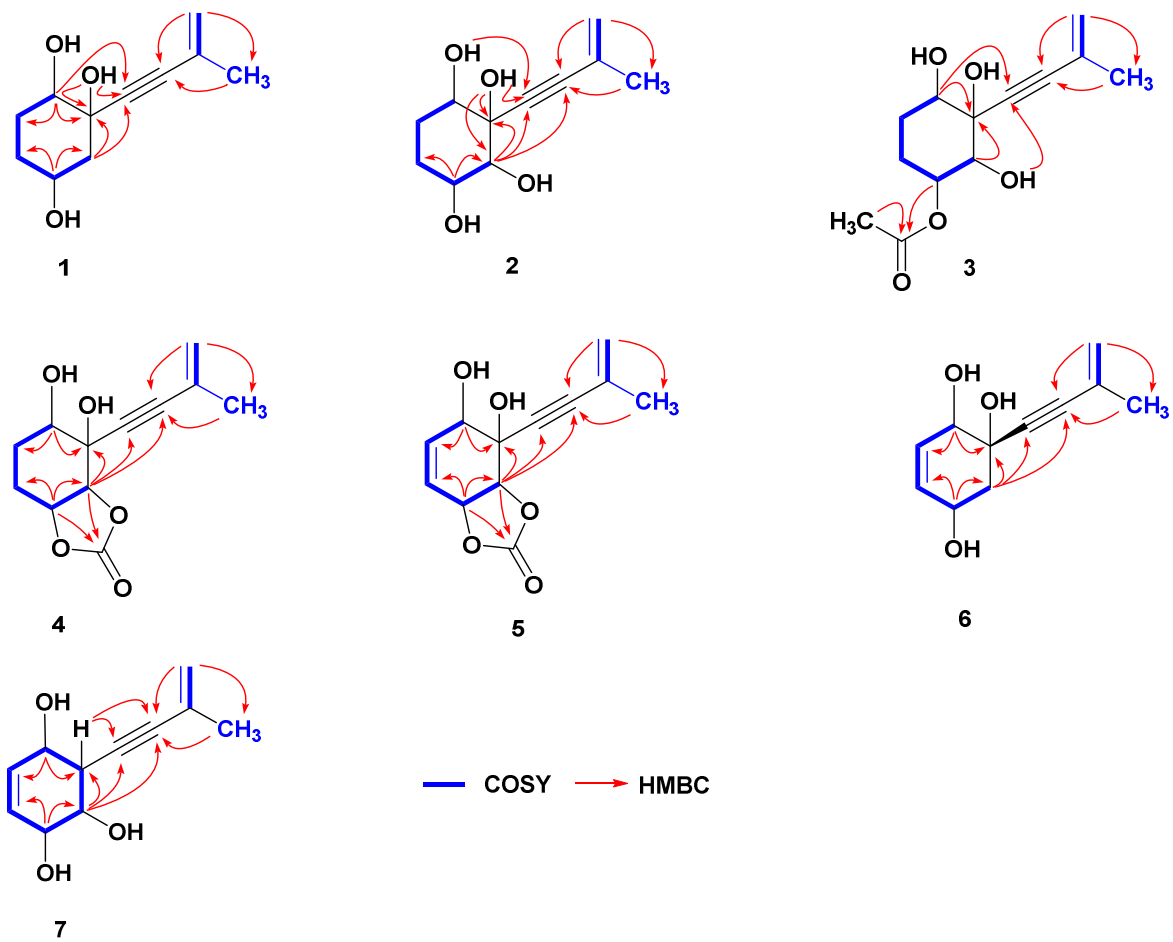


Figure 2.

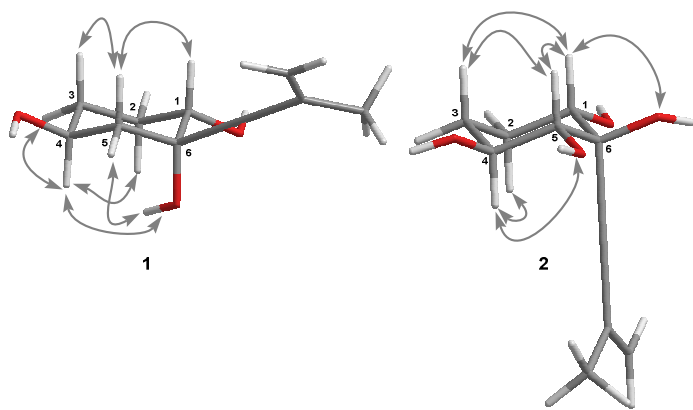


Figure 3.

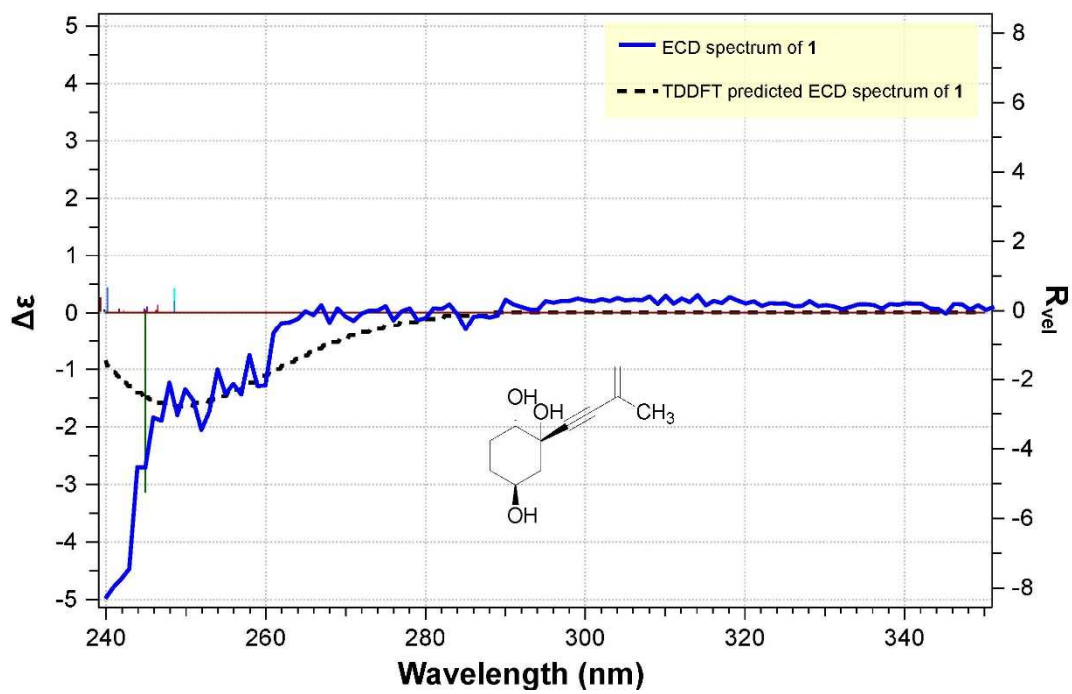


Figure 4.

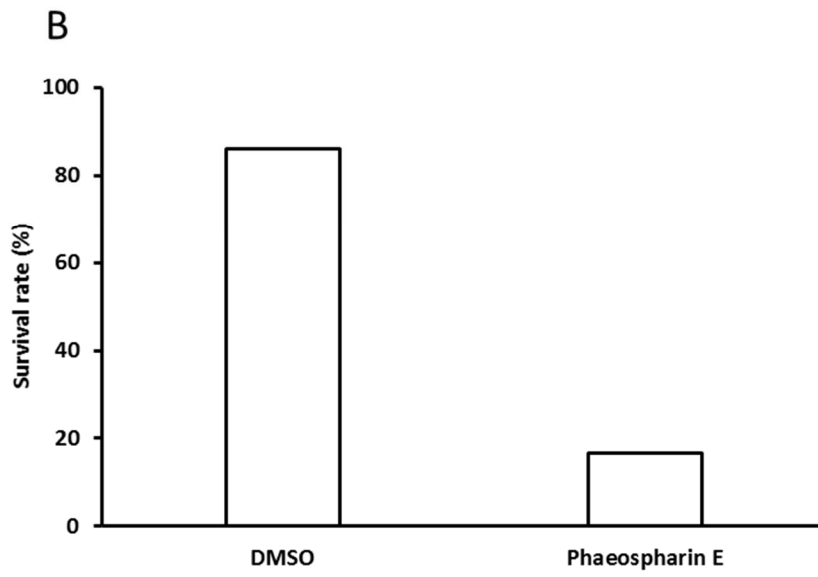
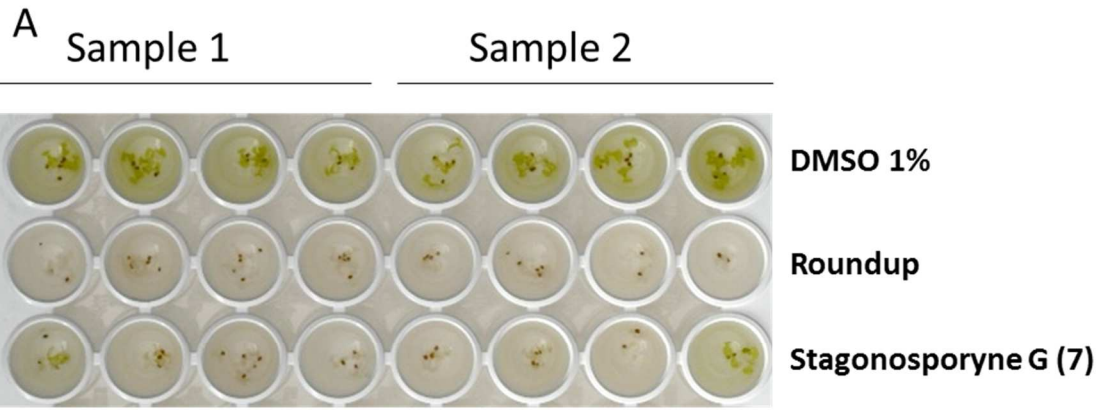


Figure 5.

Table 1.

pos.	Stagonosporyne A (1)		Stagonosporyne B (2) ^a		Stagonosporyne C (3) ^c	Stagonosporyne D (4) ^a
1	3.72, dd (10.6, 4.5) ^c	3.37, m ^b	3.46, dd (11.8, 4.4) ^a	3.27, m ^b	3.50, dd (11.8, 4.5)	3.96, dd (4.9, 1.5)
2ax	1.68, m	1.51, m	1.66, dddd (13.7, 11.8, 11.8, 4.4)	1.43, m	1.71, m	2.15, m
2eq	1.83, m		1.81, m	1.57, m	1.84, m	1.81, m
3ax	1.35, dddd (2.7, 12.7, 10.1, 3.9)	1.16, m	1.33, m	1.15, m	1.37, m	2.19, m
3eq	1.95, ddt (12.7, 6.9, 4.2)	1.71, m	1.90, m	1.67, m	1.99, m	2.02, m
4	3.97, dddd (10.1, 10.1, 4.2, 4.2)	3.60, m	3.59, ddd (11.4, 9.4, 5.0)	3.35, m	4.83, ddd (11.4, 9.9, 5.1)	4.95, m
5ax	1.66, m	1.38, m	3.17, d (9.4)	2.95, d (9.2, 4.4)	3.42, d (9.9)	4.72, d (6.5)
5eq	2.38, ddd (13.5, 4.2, 2.5)	2.06, m				
6	-	-	-	-	-	-
7	-	-	-	-	-	-
8	-	-	-	-	-	-
9	-	-	-	-	-	-
10	5.29, m	5.24, m	5.25 dq (3.2, 1.5)	5.19, br s	5.36, br s	5.31, m
	5.24, dq (3.2, 1.5)	5.19, m	5.32 dq (3.2, 1.1)	5.23, br s	5.27, br s	5.29, m
11	1.86, dd (1.5, 1.1)	1.82, dd (1.5, 1.1)	1.91, dd (1.1, 1.5)	1.82, br s	1.93, dd (1.5, 1.1)	1.86, dd (1.1, 1.5)
12	-	-	-	-	-	-
13	-	-	-	-	2.05, s	-
1-OH	2.19, br s	4.59, d (6.6)	-	4.66, d (4.3)	-	-
4-OH	2.57, br s	4.42, d (5.0)	-	4.56, d (4.4)	-	-
5-OH	-	-	-	4.85, d (4.4)	-	-
6-OH		4.89, d (1.3)		5.29, s		

a: Recorded in CD₃OD, *b*: recorded in DMSO-*d*₆, *c*: recorded in CDCl₃, *d*: recorded in CD₃CN,

Table 2.

pos.	Stagonosporyne E (5) ^a	Stagonosporyne F (6) ^a	Stagonosporyne G (7) ^a
1	4.24, d (5.0)	4.23, ddd (2.1, 2.1, 2.1)	4.20, m
2	6.24, ddd (10.1, 5.0, 1.1)	5.52, dt (10.4, 2.1)	5.64, dt (10.2, 2.0)

3	5.99, ddd (10.1, 3.5, 0.6)	5.75, ddd (10.4, 4.0, 2.1)	5.60, dt (10.2, 1.9)
4	5.30, m	4.34, m	4.03, m
5 _{ax}	4.99, d (7.4)	1.76, dd (13.3, 9.4)	3.41, dd (11.4, 8.0)
5 _{eq}	-	2.46, ddd (13.3, 5.6, 2.1)	-
6	-	-	2.62, dd (11.4, 9.3)
7	-	-	-
8	-	-	-
9	-	-	-
10	5.20-5.30, m	5.26, m	5.26-5.20, m
		5.24, m	
11	1.84, dd (1.5, 1.1)	1.88, dd (1.5, 1.1)	1.90, dd (1.5, 1.1)

a: Recorded in CDCl₃

Table 3.

pos.	1	2	3	4 ^a	5 ^a	6 ^a	7 ^a		
1	74.3, CH ^c	73.7, CH ^b	76.1, CH ^a	74.3, CH ^b	76.3, CH	73.6, CH	70.5, CH	72.8, CH	72.6, CH
2	25.9, CH ₂	27.9, CH ₂	29.4, CH ₂	28.4, CH ₂	29.1, CH ₂	24.9, CH ₂	134.7, CH	129.6, CH	132.1, CH
3	31.9, CH ₂	33.1, CH ₂	29.9, CH ₂	28.9, CH ₂	26.7, CH ₂	20.9, CH ₂	124.6, CH	133.3, CH	130.8, CH
4	65.7, CH	64.0, CH	72.6, CH	70.4, CH	75.5, CH	78.9, CH	75.5, CH	65.1, CH	73.3, CH
5	44.1, CH ₂	46.7, CH ₂	80.9, CH	79.5, CH	78.1, CH	82.9, CH	80.2, CH	44.5, CH ₂	75.6, CH
6	70.6, C	69.8, C	78.1, C	76.5, C	78.3, C	73.2, C	71.2, C	70.5, C	45.3, CH
7	89.7, C	93.8, C	87.1, C	89.3, C	86.7, C	86.7, C	86.8, C	91.9, C	88.8, C
8	85.6, C	82.5, C	89.6, C	86.5, C	90.1, C	90.1, C	89.6, C	84.7, C	84.9, C
9	125.7, C	126.5, C	128.2, C	126.7, C	128.1, C	127.6, C	127.4, C	127.9, C	128.7, C
10	122.9, CH ₂	121.4, CH ₂	122.2, CH ₂	121.1, CH ₂	122.7, CH ₂	123.4, CH ₂	123.4, CH ₂	122.15, CH ₂	121.3, CH ₂
11	23.4, CH ₃	23.3, CH ₃	23.6, CH ₃	23.4, CH ₃	23.5, CH ₃	22.9, CH ₃	23.1, CH ₃	23.1, CH ₃	23.8, CH ₃
12	-	-	-	172.7, C	157.6, C	156.5, C	72.8, CH	72.6, CH	
13	-	-	-	21.1, CH ₃	-	-	-	-	-

a: Recorded in CD₃OD, *b*: recorded in DMSO-*d*₆, *c*: recorded in CDCl₃, *d*: recorded in CD₃CN,

Figure 1: Structures of stagonosporynes A-G (**1-7**) along with siccayne (**8**)

Figure 2: Key COSY and HMBC correlations for the isolated compounds **1-7**.

Figure 3. Key NOEs for compounds **1** and **2**

Figure 4: Comparison between both experimental and TDDFT predicted ECD spectra of **1**

Table 1. ^1H NMR data δ_{H} (J in Hz) of stagonosporynes A-D (**1-4**), 600 MHz

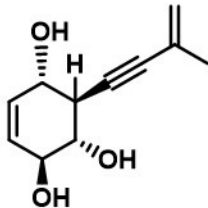
Table 2. ^1H NMR data δ_{H} (J in Hz) of stagonosporynes E-G (**5-7**), 600 MHz

Table 3. ^{13}C NMR data of stagonosporynes A-G (**1-7**), 150 MHz

Figure 5. Herbicidal activities of stagonosporyne G (**7**) at 100 $\mu\text{g/mL}$ compared to glyphosate tested at 72 $\mu\text{g/mL}$. **A)** *In vitro* toxic activity and **B)** survival rate.



Parastagonospora nodorum
SN15



Herbicidal stagonosporyne G

